Journal of Medicinal Chemistry

Article

Structure-Guided Design of EED Binders Allosterically Inhibiting the Epigenetic Polycomb Repressive Complex 2 (PRC2) Methyltransferase

Andreas Lingel, Martin Sendzik, Ying Huang, Michael David Shultz, John Cantwell, Michael P Dillon, Xingnian Fu, John Fuller, Tobias Gabriel, X. Justin Gu, Xiangqing Jiang, Ling Li, Fang Liang, Maureen Margrethe McKenna, Wei Qi, Weijun Rao, Xijun Sheng, Wei Shu, James Sutton, Benjamin Robert Taft, Long Wang, Jue Zeng, Hailong Zhang, Maya Zhang, Kehao Zhao, Mika K Lindvall, and Dirksen E. Bussiere

J. Med. Chem., **Just Accepted Manuscript** • DOI: 10.1021/acs.jmedchem.6b01473 • Publication Date (Web): 19 Dec 2016

ACS Publications

Journal of Medicinal Chemistry is published by the American Chemical Society. 1155 Sixteenth Street N.W., Washington, DC 20036

	Discovery Chemistry

Structure-Guided Design of EED Binders Allosterically Inhibiting the Epigenetic Polycomb Repressive Complex 2 (PRC2) Methyltransferase

Andreas Lingel,[‡¶*] Martin Sendzik,[‡§] Ying Huang,[†] Michael D. Shultz,[†§] John Cantwell,[‡] Michael P. Dillon,[‡&] Xingnian Fu,[†] John Fuller,[‡] Tobias Gabriel,[†¶] Justin Gu,[†] Xiangqing Jiang,[†] Ling Li,[†] Fang Liang,[†] Maureen McKenna,[‡] Wei Qi,[†] Weijun Rao,[†] Xijun Sheng,[†] Wei Shu,[‡] James Sutton,[‡&] Benjamin Taft,[‡] Long Wang,[†] Jue Zeng,[†] Hailong Zhang,[†¥] Maya Zhang,[†] Kehao Zhao,[†§] Mika Lindvall,[‡] Dirksen E. Bussiere[‡#]

[‡]Novartis Institutes for BioMedical Research, 5300 Chiron Way, Emeryville, California 94608, United States

[†]Novartis Institutes for BioMedical Research, 2418 Jinke Road, Shanghai 201203, China

Keywords:

Epigenetics, allosteric inhibition, fragment-based lead generation, oncology, EED, PRC2

Abstract

PRC2 is a multisubunit methyltransferase involved in epigenetic regulation of early embryonic development and cell growth. The catalytic subunit EZH2 methylates primarily lysine 27 of histone H3, leading to chromatin compaction and repression of tumor suppressor genes. Inhibiting this activity by small molecules targeting EZH2 was shown to result in anti-tumor efficacy. Here, we describe the optimization of a chemical series representing a new class of PRC2 inhibitors which acts allosterically via the trimethyllysine pocket of the non-catalytic EED subunit. Deconstruction of a larger and complex screening hit to a simple fragment-sized molecule followed by structure-guided regrowth and careful property modulation were employed to yield compounds which achieve sub-micromolar inhibition in functional assays and cellular activity. The resulting molecules can serve as a simplified entry point for lead optimization and can be utilized to study this new mechanism of PRC2 inhibition and the associated biology in detail.

Introduction

Polycomb Repressive Complex 2 (PRC2) is a conserved methyltransferase playing a major role in diverse biological processes such as chromatin remodeling and epigenetic silencing.[1] The core of PRC2 is composed of four proteins: EZH2 (or EZH1), EED, Suz12, and RBAP48. The SET domain of EZH2 contains the S-adenosylmethionine (SAM) dependent methyltransferase activity which catalyzes the transfer of a methyl group onto the side chain amine of lysine residues in histone tails, in particular H3K27. The enzyme can accept lysine side chains with various methylation states (non-, N-mono- and N,N-dimethylated) as substrates, resulting eventually in N,N,N-trimethylated lysines as a product (H3K27Me3 in case of H3K27 methylation). In addition to EZH2, the presence of EED and Suz12 was shown to be required for enzymatic activity.[2] This was rationalized by structural studies on the entire human PRC2[3] and minimal versions of the PRC2 containing only EZH2, EED and truncated Suz12.[4–6] These structures revealed that the three proteins form an intertwined complex in which the catalytic center is formed by EZH2 but is stabilized by domains of EED and Suz12.

Gain-of-function mutations and overexpression of EZH2 are well documented to be involved in oncogenic transformation, progression of various cancer types, as well as to be associated with poor prognosis.[7–10] Due to the link between EZH2 and cancer, multiple groups have developed small molecule antagonists to study the disease relevance, biological consequences and efficacy of inhibiting the enzymatic activity of PRC2.[11–18] All low molecular weight inhibitors reported so far are targeting the EZH2 subunit and are SAM competitive (reviewed for example by Kim et al.[19]). It has been shown that such molecules result in reduced H3K27Me3 levels and have an antiproliferative effect in both cell culture and animal models in EZH2 mutant tumors, and the first molecules are currently being evaluated in the clinic for various lymphoma indications. A

different approach to target the PRC2 activity was described by Kim et al.,[20] utilizing a stapled EZH2 peptide which is able to disrupt the EZH2-EED interface, underlining the importance of the functional interplay between these two proteins.

EED is a β-propeller protein comprised of seven WD40 repeats and was shown to directly bind EZH2 by interacting with an alpha helical peptide located at the N-terminus of EZH2 (residues 38-68) via an extended groove on one side of the propeller.[21] On the opposite side of EED, a pocket referred to as the "Me3 pocket" is selectively binding histone peptides which contain a trimethylated lysine.[22,23] An aromatic cage formed by the side chains of residues F97, Y148 and Y365 was shown to coordinate the positively charged quaternary amine of the trimethylated lysine, and the side chain of the neighboring W364 interacts with the aliphatic side chain of the lysine residue (**Figure 1a**).

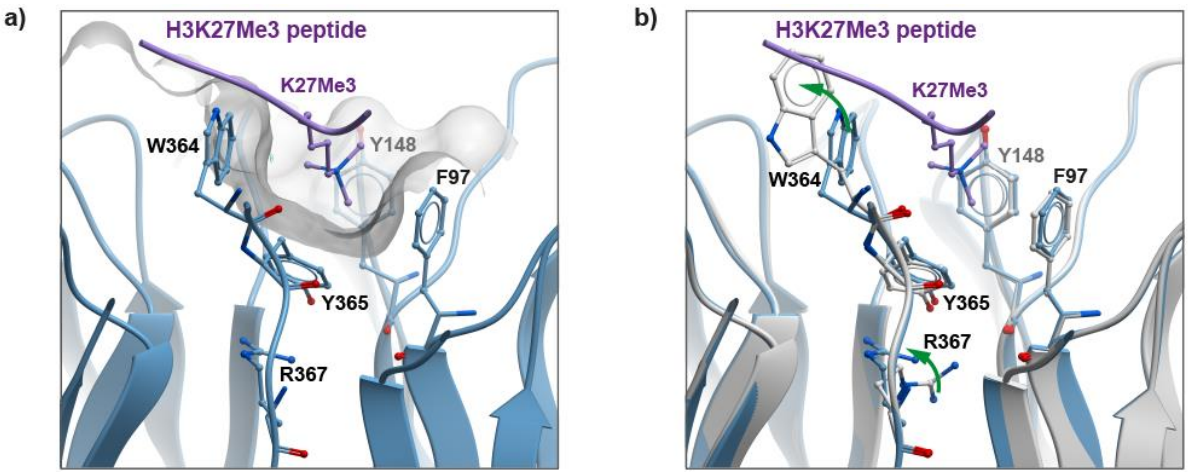

Figure 1: Interaction of the H3K27Me3 peptide with EED and associated conformational changes. (a) The X-ray co-structure of EED with H3K27Me3 peptide (PDB accession code: 3jzg) shows that the positively charged tertiary amine of K27 is located within the aromatic cage formed by EED residues F97, Y148 and Y365, and that W364 interacts with the hydrophobic part of the lysine side chain. EED is shown in blue whereas the H3K27Me3 peptide is colored purple. The protein surface around the peptide ligand is represented by a grey surface. (b) Compared to the apo EED X-ray structure (PDB accession code: 3jzn, shown in light grey), W364 undergoes a significant rotation to accommodate the peptide. In addition, the side chain of R367 rotates and forms a stacking interaction with Y365. Both movements are indicated by a green arrow.

Comparing the trimethylated lysine bound structure to the apo EED protein structure, it is found that the Me3 pocket is dynamic in nature and can undergo local conformational changes upon peptide binding. Specifically, the W364 side chain performs a rotation to accommodate the peptide ligand and the side chain of R367 moves towards F365 so that the planes of the guanidinium group and the tyrosine side chain are now oriented in parallel to form a better stacking interaction (**Figure 1b**).[23] It has also been shown that binding of trimethylated histone peptides, e.g., H3K27Me3, to the Me3 pocket allosterically activates the methyltransferase activity of PRC2.[22] Since this observation demonstrated that peptide binding to the Me3 pocket can modulate PRC2 activity, we hypothesized that a low molecular weight compound interacting with EED might display a similar effect, acting either as an activator, or more interestingly, as an inhibitor.

Herein, we report the stepwise optimization of a small molecule series with such characteristics, i.e. interacting with the Me3 pocket of EED and allosterically inhibiting PRC2 activity, representing a new mechanism of inhibition.

Results and discussion

A biochemical high throughput screening campaign to find new inhibitors of PRC2 activity led to the identification of compound **1** (**Figure 2a**).[24] Comprehensive enzymatic characterization demonstrated inhibition of PRC2 activity with a single digit micromolar IC_{50} (2.5 μM), and interestingly showed that the inhibition is non-competitive with the substrates SAM and H3K27Me0. Instead, the molecule was found competitive with the H3K27Me3 peptide, which clearly distinguishes the profile of this compound from previously described PRC2 inhibitors.[24] Based on the known interaction of EED with H3K27Me3, we explored if the competitive profile

of **1** can be explained by a direct interaction with EED. To this end, **1** was titrated onto EED protein selectively ^{13}C labeled at the terminal methyl group of methionine side chains and spectral changes assessed by 2D HSQC NMR spectroscopy. Clear, dose-dependent chemical shift perturbations of several methionine methyl resonances were observed when adding the compound to EED_{76-441} (**Figure 2b**), demonstrating a specific and localized binding event.

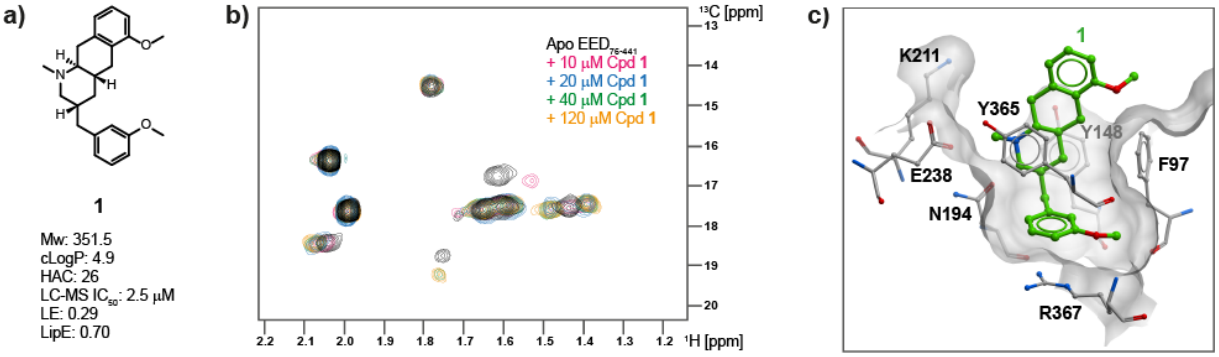

Figure 2: PRC2 inhibitor **1** is binding to the trimethyllysine pocket of EED. (a) Chemical structure, drawn in the same orientation as shown in c), and selected characteristics of the HTS hit are shown.[24] (b) Binding of **1** to isolated EED protein as detected by 2D NMR. Dose-dependent chemical shift perturbations of a subset of methionine resonances demonstrate that **1** is directly binding to EED. The spectra are colored according to the compound concentration added, as indicated in upper right corner. (c) The co-structure of EED with **1** (PDB accession code: 5H17)[24] shows that the compound is located in the Me3 pocket, with the methoxyphenyl group penetrating deepest and sitting on top of the R367 side chain, and the tertiary amine of **1** being in the aromatic cage formed by F97, Y148 and Y365.

Consistent with low micromolar affinity, the spectral changes are in the slow and intermediate exchange regime on the NMR time scale. The co-crystal structure of **1** with EED revealed that the compound binds in the trimethyllysine pocket (**Figure 1c**),[24] which is consistent with the competitive nature of the inhibitor with respect to H3K27Me3 peptide.

The protein undergoes significant local conformational changes in relationship to the apo- and peptide bound structures. This enables the compound to occupy space previously not utilized by the peptide ligand, with the methoxyphenyl moiety penetrating into the pocket and being

positioned on top of R367, and the positively charged piperidine moiety of the tricyclic core of **1** located within the aromatic cage. The rest of the molecule is mainly solvent exposed and does not seem to participate in major interactions.

Due to the high complexity of compound **1** and the associated synthetic challenges in exploring SAR, our first goal was to investigate the key chemical moieties for EED activity and thereby identify smaller as well as simpler molecules that were substructures of **1**. This approach of ligand deconstruction[25,26] has the potential of identifying "minimal pharmacophores" or minimal fragments which can be regrown more efficiently to improve potency and other properties in ways that were not originally accessible from the parent molecule. Here, the crystal structure enabled deconstruction of **1** in the middle of the tricyclic ring – an unusual approach as ring systems are usually considered "cores" and are typically not broken – and pointed to a commercially available compound **2** (**Figure 3a**) as the more buried and likely more relevant half of **1**. Compound **2** showed direct binding to EED in the 2D NMR assay with a K_D of 32 µM and induced chemical shift perturbations of the same resonances perturbed by **1** (Figure S1 in the Supporting Information), as well as inhibiting PRC2 activity with an IC_{50} of 95 µM. Despite the decrease in biochemical potency, ligand efficiency (LE) and lipophilic efficiency (LipE) were increased by 0.07 from 0.29 (**1)** to 0.36 (**2**) and by 0.52 from 0.70 (**1**) to 1.22 (**2**), respectively. The co-crystal structure of **2** with EED (data and refinement statistics are presented in Table S1 in the Supporting Information) shows that the interactions made with the protein are the same as the ones observed for the parent compound **1** (**Figure 3b**) and that the binding pose is completely retained (**Figure 3c**). This structural data, combined with the efficiency improvements noted above, suggests that molecule **1** was successfully deconstructed to a minimal pharmacophore **2** that efficiently engages with the Me3 pocket even though the absolute potency decreased.

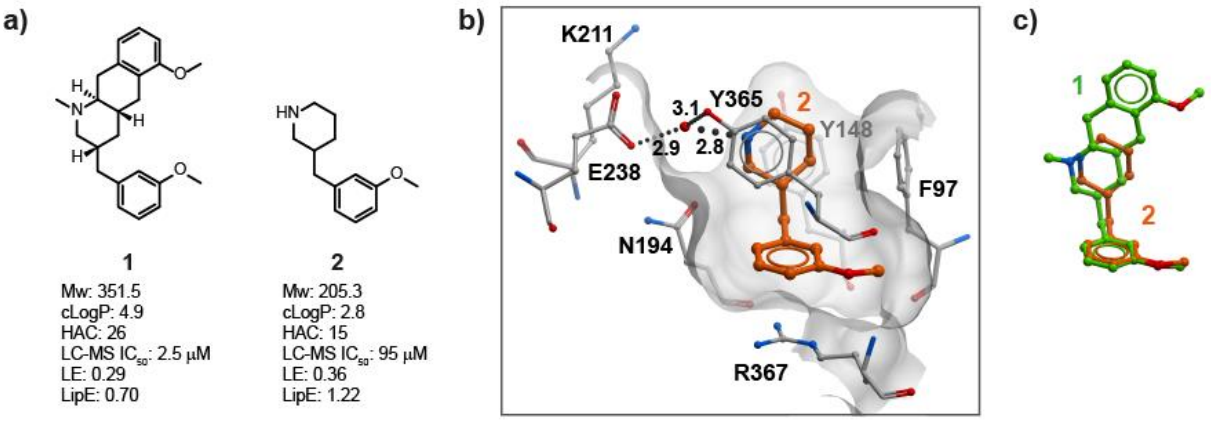

Figure 3: Deconstruction of **1** yields compound **2** which retains binding mode and critical interactions. (a) Chemical structures, drawn in the same orientation as shown in c), and selected characteristics of **1** and **2** are shown. (b) The co-structure of EED with **2** (PDB accession code: 5U5K) shows that compound **2** is located in the same position in the Me3 pocket where the parent compound **1** was found. The piperidine amine is positively charged and located inside the aromatic cage, whereas the methoxyphenyl group is stacking with R367. A structured water bridges interactions with N194 and Y365. (c) Overlaying the co-structures of EED with **1** and **2** shows that the bound state of **1** (green) and **2** (orange) are highly similar and equivalent atoms are in almost identical positions.

The methoxyphenyl moiety is deeply buried inside the protein and is forming a pi-positive charge stacking interaction with the guanidinium group of R367. We refer to this part of the binding site as the "deep pocket". The side chain of R367 is involved in a similar interaction with Y365 in the apo-structure of the protein, and an outward movement of Y365 provides the required space to accommodate the compound (**Figure 4a**).

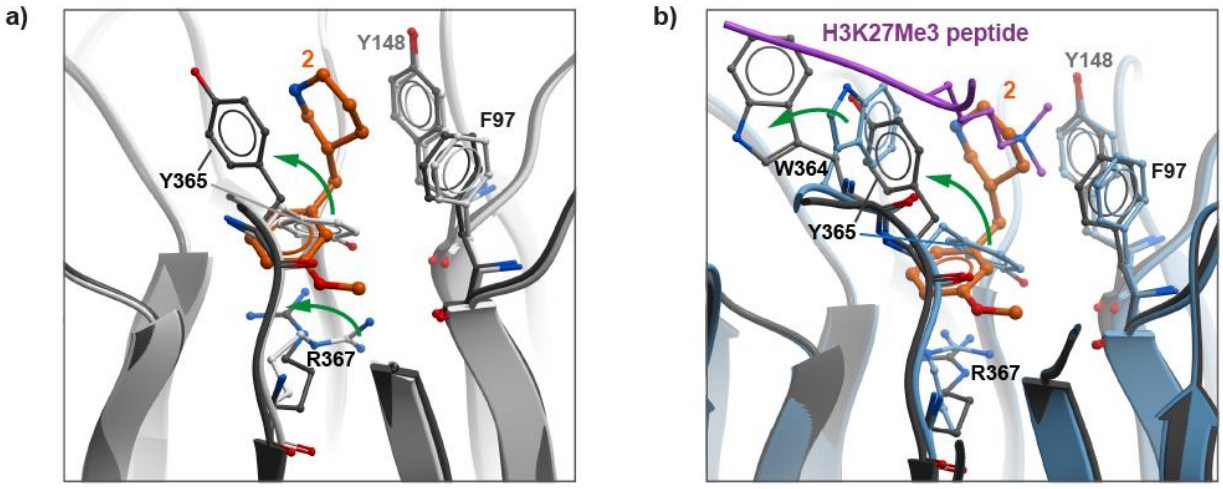

Figure 4: Conformational changes observed upon binding of compound **2**. Colors are corresponding to Figure 1 and Figure 2. (a) Overlay of the apo EED X-ray structure (PDB accession code:3jzn) with the X-ray co-structure of EED with compound **2 (**PDB accession code: 5U5K). Y365 swings out which results in the formation of the "deep pocket" occupied by the methoxyphenyl moiety of compound **2**, whereas R367 rotates towards the compound to form a pi-positive charge stacking interaction. Both movements are indicated by green arrows. (b) Overlay of the X-ray co-structure of EED with H3K27Me3 peptide (PDB accession code: 3jzg) with the X-ray co-structure of EED with compound **2 (**PDB accession code: 5U5K). W364 rotates out to a location which is occupied by the peptide backbone in the peptide complex. The large movement of Y365 results in a relocation of the aromatic cage, so that the positively charged piperidine moiety of **2** is shifted compared to the tertiary amine of lysine 27 of the H3K27Me3 peptide. Both movements are indicated by green arrows.

The ligand moiety in the deep pocket is entirely surrounded by protein, with some space available in the ortho-position next to the meta-methoxy group, but not in the para-position. The piperidine ring is located in the aromatic cage formed by Y365, Y148 and F97. Interestingly, the charge-bearing nitrogen in the piperidine ring is positioned in the same location as the quaternary amine of the peptide ligand methylated lysine. This suggests that the small molecule ligand is recapitulating the cation-pi interaction of aromatic cages (**Figure 4b**). The two tyrosine side chains are oriented parallel to the piperidine ring, whereas the phenylalanine is oriented perpendicular. As seen for **1**, the methylene linker between the methoxyphenyl group and the

piperidine in compound **2** provides a turn to the molecule and enables the placement of the two moieties in the respective subpockets (**Figure 3b**).

Consistent with of our overall drug discovery efforts on EED,[27] we pursued a stepwise strategy in modifying the compound starting in the deep pocket and then moving towards the aromatic cage with the goal of simultaneously improving potency, LE and LipE values.

Potency enhancement through modifications of the moiety in the deep pocket

Based on the observation that the methoxyphenyl group is stacking with the guanidinium group of the R367 side chain and considering the associated attractive forces between the electron-rich aromatic system and the delocalized positive charge, we initially investigated the effect of the methoxy group. Removing the methoxy group resulted in a compound without detectable potency (**3**, **Table 1**), while substituting the ortho-position (**4**) led to similar potency. Moving the methoxy group to the para position was accompanied by significant potency loss (**5**, **Table 1**). These results are consistent with structural analysis of available space obtained from the co-crystal structure, as described above.

Table 1: Molecules of the amine series: Initial optimization of the moiety in the deep pocket

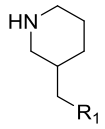

Compound	R_1	IC_{50} [µM]	LE[1]	cLogP	LipE[1]
2	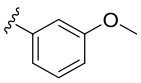	95	0.36	2.8	1.22
3		> 500	< 0.35	2.9	< 0.40
4	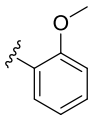	146	0.35	2.8	1.04
5	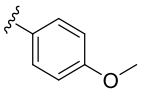	> 500	< 0.30	2.8	< 0.50
6	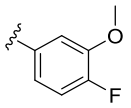	119	0.33	2.9	1.02
7	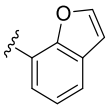	95	0.34	3.4	0.62
8	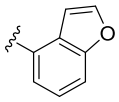	40	0.37	3.4	1.00
9	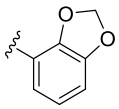	35	0.38	2.8	1.66

[1]LE and LipE values are calculated according to LE=1.36*pIC_{50}/HAC and LipE=pIC_{50}-cLogP, respectively.

Introduction of fluorine next to the meta-methoxy group at the para-position (**6**) did not significantly alter the potency, indicating that fluorine is small enough to be tolerated in this location. While we hypothesized that the fluorine might be able direct the neighboring methoxy

group into an orientation consistent with the conformation observed in the crystal structure of **2,** the lack of improvement might be a result of competing electronic effects.

Following the previous observations, we next explored the possibility of filling the observed space by introducing a second ring fused to the phenyl ring at the ortho- and meta-position, while keeping oxygen containing groups. Introduction of benzofuran or benzodioxole moieties, linking the substituents of the methoxy compounds in the ortho- and meta-position, demonstrated that a moderate but consistent two-fold increase can be achieved (**7**, **8**, and **9**). The two benzofuran regioisomers (**7**, **8**) behave consistent with the methoxyphenyl compounds (**3**, **4**) with the meta-O-substitution slightly preferred. The benzodioxole (**9)** displays potency comparable to **8** (**Table 1**).

Modifications of the moiety localized within the aromatic cage

The secondary amine of the piperidine ring in **2** is positively charged (with a measured pK_a of 9.9) and positioned in the aromatic cage, similar to the trimethylated lysine side chain in the EED-H3K27Me3 co-crystal structure. Additionally, the amine participates in a hydrogen bond network with a structured water and polar groups of the side chains of surrounding amino acids (**Figure 3b**). Thus, the interactions within this subpocket are expected to be significant contributors to potency and could provide a great potential for optimization. Prospective optimization of cation-pi interactions and pi-pi interactions is challenging using conventional computational methods employed for compound assessment, such as docking with scoring functions and structure-based affinity predictions. Therefore, we decided to apply an experimental approach and synthesized molecules with moieties sampling different possible concepts of interaction with the cage, while retaining the moieties in deep pocket. We evaluated

three concepts: a point charge, a delocalized charge combined with an aliphatic pi system, and a delocalized charge combined with an aromatic system (**Figure 5**).

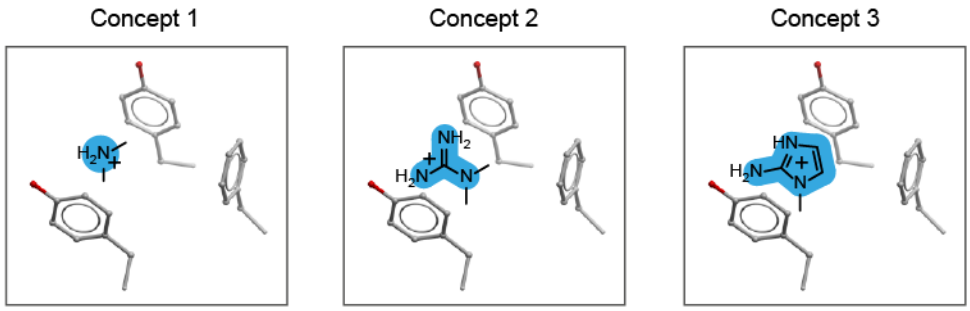

Figure 5: Design concepts for different moieties located in the aromatic cage. The side chain of F97, Y184 and Y365, forming the aromatic cage of EED, are shown. An example chemical structure of a moiety representing the respective concept is shown inside the cage with the area of the blue color representing the localization of the charge.

Concept 1 was explored by the HTS hit and its deconstructed analog **2**. Our design efforts towards concept 2, combining a delocalized charge with a pi stacking interaction, yielded amidines and guanidines with different substitution patterns and ring closures. One example is the guanidinium containing compound **10** (**Table 2**), which has a measured pK_a of >11 and shows a two-fold improvement in IC_{50} compared to the parent compound **2,** despite an anticipated dehydration penalty. Next, we combined the new guanidinium containing moiety in the aromatic cage with moieties previously characterized in the deep pocket (**Table 2**). A combination with the benzofuran group resulted in compounds **11** and **12**, which had single digit micromolar potency in the biochemical assay, showing that improvements arising from changes in the two sub-pockets were not simply additive in nature. To evaluate if the improvement observed going from the piperidine to the guanidinium was due to the charge or potential pi-pi interactions, we tested the corresponding urea analog (**13**) and found that the potency dropped by

approximately 80 fold, demonstrating the importance of the positive charge in the aromatic cage in the context of this series. An improvement to single digit micromolar potency was also observed for the previously identified benzodioxole analog (**14**, **Table 2, Figure 6a**). In addition to the enhancements in potency, we also observed improvement in efficiency parameters, in particular LipE as a result of the guanidinium group (e.g., a LipE of 3.51 of compound **14** compared to 1.66 of compound **9**).

Table 2: Molecules of the guanidinium series

Compound		IC_{50} [µM]	LE[1]	cLogP	LipE[1]	G-401 ELISA IC_{50} [µM]
10	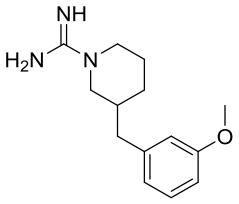	43	0.33	1.9	2.47	n.d.
11	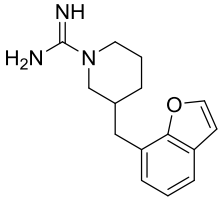	2.8	0.40	2.5	3.05	2.5
12	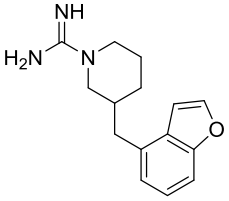	2.1	0.41	2.5	3.18	2.5
13	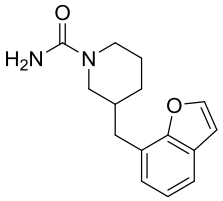	174	0.27	1.7	2.06	n.d.
14	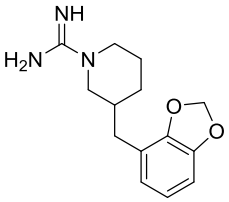	3.9	0.39	1.9	3.51	1.6

[1]LE and LipE values are calculated according to LE=1.36*pIC$_{50}$/HAC and LipE=pIC$_{50}$-cLogP, respectively.

A co-structure of EED and **14** (**Figure 6b,** Table S1 in the Supporting Information), combining improvements in the two sub-pockets, shows that the benzodioxole moiety is placed on the R367 side chain and that the position of the phenyl ring is completely retained with respect to **2** (**Figure 6c**).

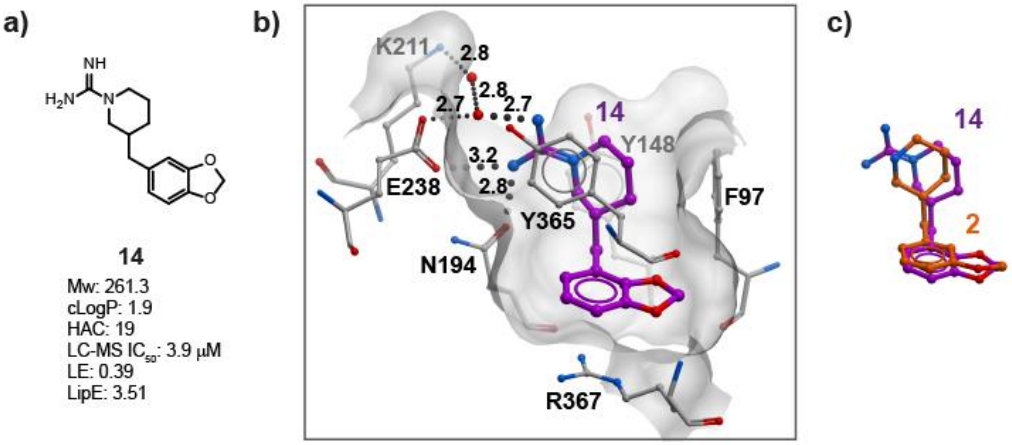

Figure 6: Co-structure of **14** with EED **(**PDB accession code: 5U5T). (a) Chemical structure and selected characteristics of **14** are shown. (b) The guanidinium group of **14** interacts directly with the side chains of N194 and E238 and via a structured water with E238. (c) The overlay of the co-structures of EED with **2** (orange) and **14** (magenta) shows that the compounds adopt a highly similar binding mode.

The charged guanidinium group is replacing a water molecule and is positioned to interact directly with the side chains of N194 and E238. In addition, a water molecule bridges an interaction to the second oxygen of E238.

Having reached the single digit micromolar potency level in the functional assay with compounds **11**, **12,** and **14**, we decided to test these compounds for activity in a cell-based assay using a proximal marker. The respective assay reads out the cellular methylation status of K27 of histone 3 in G-401 cells, which are rhabdoid tumor cells of kidney origin known to be dependent on PRC2 and therefore sensitive to PRC2 inhibitors.[15,28] The detection of H3K27Me3 is

performed by ELISA, and we refer to the assay as the G-401 ELISA assay. We found that the compounds were able to inhibit H3K27 methylation in cells with an IC_{50} of approximately 2 μM (**Table 2**), demonstrating that compounds inhibiting PRC2 through binding to EED result in the same cellular readout as previously described for EZH2 inhibitors. Interestingly, the IC_{50} values observed in the biochemical and cellular assays are comparable for several of these compounds, despite limited permeability (see below), which could be a result of their allosteric mechanism of inhibition.

Property improvement

While we achieved cellular activity with molecules of the guanidinium series, the guanidinium group is generally not preferred because the strong positive charge often negatively impacts cell permeability. Indeed, when comparing Caco-2 data of representative examples of the piperidine series (**8**, pK_a of 9.8) and the guanidinium series (**12**, where the very close analog **14** has a pK_a of >11), we observe a 15-fold drop in permeability from 34.3 to 2.3 10^{-6} cm/s (Table S2 in the Supporting Information). Therefore, we next explored design concept 3 which retained a positive charge – now delocalized in an aromatic pi system (**Figure 5**) – while lowering the pK_a value. Such chemical moieties were more challenging to identify by informatics, because pK_a predictions for such less frequently used systems may not be reliable and databases of pK_a measurements do not typically annotate where the ionization center is located. Searching of the BioLoom database[29] for measured pK_a values of 8 or greater, combined with substructure searching for aromatic atoms and ascending sorting by molecular weight, identified top scoring entries where a basic pK_a was typically in the context of an aromatic ring, including 4-

aminopyridine (average pK_a of 9.1) and 2-aminoimidazole (pK_a of 9.2 with 4,5-dimethyl substitution).

We decided to explore the 2-aminoimidazole moiety (**15**, **16**, **Table 3**), as it might allow simultaneously improving the physico-chemical properties of the series by mitigating the high pK_a, decreasing the number of H-bond donors and rotatable bonds, as well as PSA, while keeping all observed interactions. Compound **16** has a measured pK_a of 9.2 – significantly lower than the corresponding guanidinium (**14**) with pK_a of >11 – showing that it retains the positive charge and is therefore a suitable moiety. Accordingly, molecules of the aminoimidazole series show good permeability, as exemplified by compound **15** (16.8 compared to 2.32 10^{-6} cm/s for compound **12**, and 25.6 10^{-6} cm/s for compound **16**, Table S2 in the Supporting Information). In addition, the IC_{50} of these aminoimidazole analogs approaches the 1 µM mark and they showed cellular activity (**Table 3**).

Table 3: Molecules of the aminoimidazole series.

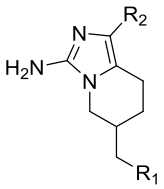

Compound	R_1	R_2	IC_{50} [µM]	LE[1]	cLogP	LipE[1]	G-401 ELISA IC_{50} [µM]
15	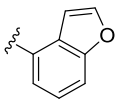	H	2.7	0.38	3.0	2.57	12.4
16	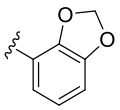	H	1.3	0.40	2.5	3.39	1.0

17	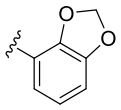	isopropyl	0.43	0.38	3.6	2.77	2.0
18		isopropyl	7.9	0.33	3.8	1.30	n.d.
19	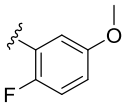	isopropyl	1.3	0.35	3.9	1.99	2.9

[1]LE and LipE values are calculated according to LE=1.36*pIC$_{50}$/HAC and LipE=pIC$_{50}$-cLogP, respectively.

The co-structure of **16** (Table S1 in the Supporting Information) confirmed that the aminoimidazole group is replacing the guanidinium group and that the amine is engaged in water-mediated interactions with N194 and E238 (**Figure 7b**). Interestingly, direct binding to N194 and E238 was lost and previously observed water-mediated interactions were regained.

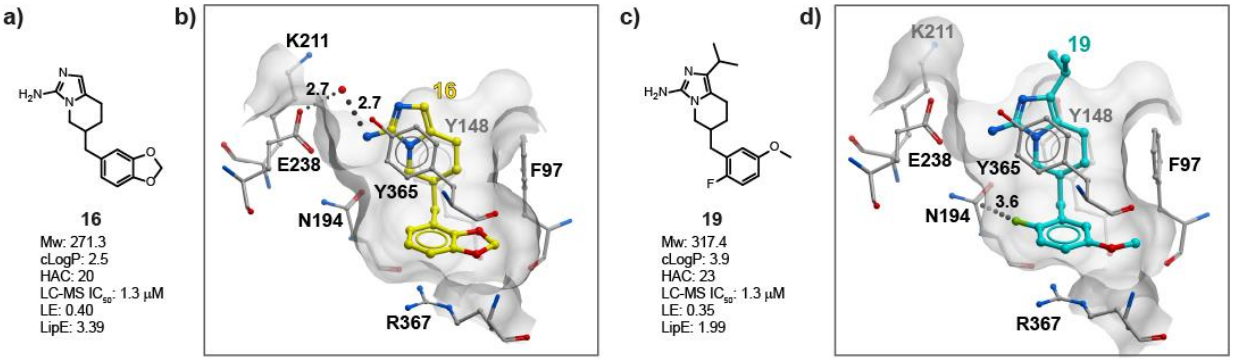

Figure 7: Co-structures of EED binders with improved properties **(**PDB accession codes: 5U62 and 5U5H). (a) Chemical structure and selected characteristics of **16** are shown. (b) The 2-aminoimidazole group in **16** acts as an effective replacement for the guanidinium group in **14** with improved properties. (c) Chemical structure and selected characteristics of **19** are shown.

(d) The binding mode of the ortho-fluoro meta-methoxyphenyl moiety of **19** is similar to the one observed for the benzodioxole group. The fluorine points towards the side chain amide of N194.

To evaluate growth opportunities on the imidazole ring, we introduced aliphatic groups (e.g., isopropyl, **17**) at the 4-position, achieving sub-µM activity in the functional assay (**Table 3**) and an IC_{50} of 2 µM in the cell-based G-401 ELISA assay.

Encouraged by this result, we tested compound **17** also in a cell proliferation assay monitoring the effect of the compound on the growth of Pfeiffer cells, which are B lymphocytes and EZH2 mutant, making them sensitive to PRC2 inhibitors.[11,12] Using **17**, we observed a dose-dependent anti-proliferative effect with an EC_{50} of 3.4 µM, demonstrating that compounds targeting the EED Me3 pocket not only lead to a reduction of the cellular H3K27 methylation level, but also have a direct effect on cell growth, as previously seen for EZH2 inhibitors.

In an additional optimization step, we re-investigated the moiety in the deep pocket in the presence of the aminoimidazole ring system to mitigate potential liabilities presented by the aromatic system with high electron density. Based on the available structural information, we introduced fluorine at the ortho-position, which could make a possible interaction with neighboring backbone or side chain amide groups (e.g., N194),[30] and prepared corresponding analogs (**18**, **19**, **Table 3**). Compound **18**, which contains only an ortho-substituted fluorine on the phenyl ring, retains single digit micromolar affinity, demonstrating approximately 100-fold increase in potency compared to the early phenyl/piperidine-derivative **3.** We generally observed a two-fold boost in potency when introducing the ortho-fluorine. The ortho-fluoro meta-methoxy substituted compound **19** (**Figure 7c**) displays biochemical potency at the 1 µM level, an IC_{50} of 2.9 µM in the G-401 ELISA assay and an EC_{50} in the cell proliferation assay of 4.4 µM.

In order to assess if these more advanced compounds of the series still act by the same mechanism observed for the original screening hit,[24] we performed equivalent enzymatic studies with compounds **16** and **19** (Figure S2 in the Supporting Information). These experiments showed a non-competitive profile with SAM and H3K27Me0, but a competitive profile with H3K27Me3, confirming the expected mechanism of inhibition.

Solving the X-ray co-structure of EED with **19** (**Figure 7d**, Table S1 in the Supporting Information) showed that the location of the methoxyphenyl group is retained and that the fluorine atom is pointing towards N194, indeed making a positive interaction with the side chain amide as designed, with a distance of 3.6 Å to the amide carbon atom. While we haven't explored the 4-position of the aminoimidazole moiety further thus far, the isopropyl group is pointing towards the solvent, indicating that this vector is available for further optimization in the future.

Conclusions

Although inhibition of PRC2 activity was shown to result in a decrease of H3K27 methylation levels as well as inhibition of cell proliferation and *in vivo* efficacy in lymphoma mouse models, so far EZH2-directed molecules are the only class of small molecule inhibitors described in the literature. While these molecules are currently being evaluated in the clinic, recent studies report target mutations in WT or mutant EZH2 to occur after prolonged dosing, resulting in resistance to EZH2 inhibitors.[31,32] Because all currently known inhibitors act via the same mechanism, this raises the potential that such and similar mutations could affect their ultimate efficacy. Therefore, inhibitors acting by a different mode of inhibition are highly valuable, due to the different resistance profile and potential synergistic effect with known inhibitors.

In this study, we have described a small molecule series binding to the Me3 pocket of the PRC2 subunit EED and leading to inhibition of the methyltransferase activity. This mode of inhibition is allosteric in nature, in contrast to the orthosteric, SAM-competitive EZH2 inhibitors. Interestingly, binding of the natural H3K27Me3 peptide ligand to the Me3 pocket allosterically activates PRC2 activity, and this agonistic effect was hypothesized to facilitate spreading of the repressive mark along the chromatin.[22] In contrast, the described compounds act antagonistically through the same pocket. We believe that the inhibition is a result of two mechanisms: First, blocking the Me3 pocket with an inhibitor prevents proper localization of PRC2 to chromatin with existing H3K37Me3 marks. Second, interaction of the compound with the Me3 pocket is directly inhibiting the methyltransferase activity by an allosteric mechanism. By analyzing the available crystal structures of EED in isolation, we were not able to decipher the molecular basis for this phenomenon. However, the recently reported crystallographic systems containing the PRC2 core components EZH2, EED and Suz12[4,5] will help to explain the molecular basis of this new mechanism.

Our chemistry strategy involved deconstruction of a HTS hit (**1**) to a substructure representing half of the parent molecule (**2**). While the screening hit was a structurally complex molecule and synthetically challenging to access, the resulting fragment featured greatly reduced complexity as well as higher synthetic tractability and therefore represented a better starting point for chemistry optimization. Biophysical and structural validation confirmed a retained binding mode and fragment-based drug discovery principles confirmed success in deconstruction: for even though potency was reduced, ligand efficiency and lipophilic efficiency increased (Figure S3 in the Supporting Information). The less complex starting point enabled a stepwise optimization in a way that would not have been possible from the more complex tricyclic HTS hit and yielded an

optimized fragment with further increased ligand efficiency parameters (**14**, Figure S3 in the Supporting Information). The optimized fragment allowed us to validate activity in cell-based assays, demonstrating that a similar outcome observed for EZH2 inhibitors can be achieved with an EED binder which provided confidence to pursue this approach and to start improving properties. Replacing the guaninidinium group with the aminoimidazole moiety significantly improved permeability while maintaining good efficiency and cell-based activity. We also established a vector available for property modulation and potency improvement, and introduced a moiety in the deep part of the pocket that is more drug-like without significant potency loss (**19**). Together, these changes led to a decrease in efficiency parameters, a phenomenon often observed when going beyond the initial optimization phase towards lead optimization, but to a simpler, tractable and more efficient molecule when compared to the HTS hit. The resulting molecules can be further optimized and can serve as tool compounds to study the biology of EED-mediated inhibition of PRC2 activity.

Experimental Section

Complete information on material and methods can be found in the Supporting Information.

Protein expression and purification. PRC2 (containing human EZH2, Suz12, EED, RBAP48 and AEBP2 proteins) used in the biochemical assay was expressed in insect cells and purified as described previously.[15] Human EED protein (residues 76–441, Uniprot ID O75530) was produced in *E. coli.* BL-21 (DE3) CodonPlus cells which were transformed with a pDEST14 (Life Technologies) plasmid containing the His_6-TEV-EED_{76-441} construct. Unlabeled protein was expressed in cells grown in LB medium, whereas selectively methionine-$^{13}C\varepsilon$ labeled

protein for NMR studies was produced in minimal media supplemented with 250 mg/L L-methionine-(methyl-^{13}C) and various amounts of the other 19 amino acids. Proteins were purified by IMAC using a Ni column followed by size exclusion chromatography.

NMR binding assay. 2D [^{13}C, ^{1}H]-HSQC experiments were recorded on a Bruker NMR spectrometer at 600 MHz ^{1}H Larmor frequency equipped with a 5 mm QCI cryogenic probe at 296 K. Samples contained 40 µM selectively methionine-^{13}Cε-methyl labeled EED_{76-441} protein in 25 mM d-Tris pH 8, 150 mM sodium chloride, 2 mM d-DTT, and 10% D_2O. K_D values were determined by titrating EED protein with increasing amounts of ligand and following the resulting chemical shift perturbations.

X-ray crystallography. The crystal co-structures of EED_{76-441} with compounds **2** and **19** were determined using crystals grown in a precipitant composed of 3–3.5 M sodium formate[22,23] using the vapor diffusion method. Crystals grew in 3–5 days at 18 ºC and harvested and soaked in defined drops consisting of 30 µL of precipitant with 1–2 mM of compound (typically solubilized in DMSO) for 24–48 h. Crystals were cryopreserved for data collection using a cryosolution consisting of 3.5 M sodium formate, 1–2 mM of compound, and 30% (v/v) glycerol.

The crystal co-structures of EED with compounds **14** and **16** were determined by using a PEG/salt combination as a precipitant. Briefly, EED was incubated with 10 mM β-nicotinamide adenine dinucleotide hydrate, 2 mM of a tightly binding proprietary compound, and 0.5 mM of a synthesized peptide which comprises the helix on EZH2 which interacts with EED.[21] The crystals were grown using the vapor diffusion method. 1 µL of the protein mixture was combined with 1 µL of a precipitant comprised of 20% (w/v) PEG3350, 0.2 M potassium iodide,

and 0.1M Tris-HCl, pH 8.5, on a cover slip which was suspended over a reservoir comprised of 0.5 mL of precipitant at 18 ºC and sealed. The crystals grew in 4–6 days at 18 ºC and then harvested and soaked in defined drops consisting of 30 µL of precipitant and 2 mM of compound for 24 h. Crystals were cryopreserved for data collection using a cryosolution consisting of 30% PEG 400 (v/v), 20% (w/v) PEG 3350, 0.2 M potassium iodide, and 0.1M Tris-HCl, pH 8.5. Structures were solved by molecular replacement using the structure of a previously determined apo EED structure with or without the EZH2 peptide as warranted. The coordinates were refined to convergence using *COOT*,[33] *BUSTER*,[34]and the *PHENIX*[35] suite of programs. Data collection and refinement statistics for all structures are given in Table S1 in the Supporting Information.

Biochemical assay. Inhibition of PRC2 activity was measured by quantification of the co-product SAH by LC-MS, as described.[15,36] Briefly, PRC2 (10 nM) was incubated with co-factor SAM (1 µM, at K_m) and substrate histone H3[21–44, K27Me0] peptide (1.5 µM, at K_m) as well as test compound at various concentrations (with a top concentration of either 50 mM or 10 mM and three-fold serial dilutions to a total of 12 points) in assay buffer (20 mM Tris-HCl, pH 8.0, 0.01% Triton X-100, 0.5 mM DTT and 0.1% BSA). After incubation of the reaction for 2 h at r.t., the reactions were stopped by adding 2.5% TFA and 320 nM SAH-d_4. The amount of SAH produced from the reactions was measured using an API4000 liquid chromatography/tandem mass spectrometry (LC/MS/MS) system. SAH-d_4 was used as an internal standard (IS) for SAH detection and normalization. The plot of SAH peak area/IS peak area *versus* SAH concentration was used to generate the normalization factor of SAH. The production of SAH from the enzymatic reaction was derived from the standard curve of SAH. The detection limit of our system for SAH is approximately 1 to 2 nM, and the range is linear up to 400 nM. All

measurements were run in duplicates and IC_{50} values were highly reproducible. The reported values are qualified IC_{50} values and not absolute IC_{50} numbers, since 50% inhibition was not always achieved with the test compounds in the early phase of the optimization. In addition, we made a general observation that the maximum achieved inhibition varies and doesn't consistently reach 100%, which could be a result of the allosteric mechanism.

Cell-based assays. Cells were maintained in a humidified incubator at 37 °C, 5% CO_2 (v/v). The effect of the compounds on the cellular H3K27 methylation status was assessed in G-401 cells (ATCC CRL-1441). Cells were seeded in 384 well plates and cultured for 24 h before treatment with serial dilution of compounds. A DMSO control containing the same volume percentage of DMSO was also included. After incubation for 48 h, cells were washed with phosphate based buffer (PBS, pH 7.4) twice and lysed by adding lysis buffer (0.4 N HCl; 45 µl per well). After gentle agitation for 30 min at 4 °C, neutralization buffer (0.5 M sodium phosphate dibasic, pH 12.5, Protease Inhibitor Cocktail, 1 mM DTT; 36 µl per well) was added to the wells. The plate was agitated again, followed by transfer of a 10–15 µL aliquot of the cell lysates to a 384 well ELISA plate. After overnight incubation at 4 °C, the wells were washed with TBST 5 times, and TBST was completely removed after each wash using a paper towel. After blocking with blocking buffer (TBST with 5% BSA) for 1 h at r.t., the primary antibody was added in blocking buffer, and the plate was incubated for 1 h at r.t. After washing again, ECL substrate was added and the plates were centrifuged at 2,000 rpm for 2 min. The signal was read using a PerkinElmer Envision Reader. Percentage inhibition was calculated against the DMSO control after normalization of the H3K27Me3 signal to the H3 signal for individual

samples. The data were then fit to a dose response curve to get the IC_{50} values of the test compounds.

Compound-dependent inhibition of cell proliferation was assessed in exponentially growing Pfeiffer cells (ATCC CRL-2632) in 384 well plates. After 6 days of compound incubation, CellTiter-Glo reagent (CTG reagent, Promega G7573) was used for cell growth measurement. The luciferase signal was read using a PerkinElmer Envision Reader, the percentage inhibition was calculated against a DMSO control and IC_{50} values determined by fitting the inhibition curves.

Determination of pK_a values. Calculated pK_a values were determined with the program *MoKa* (Molecular Discovery). Experimental pK_a values were determined by the capillary electrophoresis method and potentiometric method, as described previously.[37]

Caco-2 assay. Caco-2 permeablity measurements were performed on 21 day Caco2 cell cultures. Plates were washed of cell media by aspirating the full volume (75 µL apical, 250 µL basolateral) and replacing it with warmed Caco2 Transport Buffer three times. The compound source plate was prepared in a 2 mL deep well block. 4 µL of each compound (at 4 mM in DMSO) was added to each well, followed by the addition of 1.6 mL of transport buffer to each well resulting in a compound concentration of 10 µM. After aspirating the full volume of buffer in the apical transwell, compounds are dosed in triplicate in the forward (A-B) and reverse (B-A) directions. For time point 0 (t0), 10 µL is aspirated from each donor well and added to 30 µL of transport buffer in the analytical plate The dosed transwell plates were then incubated at 37 ºC with humidity and shaking at 180–240 rpm for 2 h. After incubation, 40 µL aliquots from

receiver wells and 10 µL aliquots from apical wells (for recovery calculation) were collected from all wells of the transwell plate. Next, 40 µL of mobile phase (80% water, 20% methanol, 0.3 ng/mL glubiride (internal standard)) was added to all wells of the analytical plate. Each well of the analytical plate was analyzed by LC/MS/MS (Waters UPLC system combined with an ABI 4000 Qtrap Triple Quad Mass Spectrometer) running in MRM mode for compound and the internal standard. The apparent flux (P_{app}) for each well is calculated as follows: P_{app} = (dQ/dt)*(1/C0)*(1/A) where dQ/dt is the transport rate, C0 is the compound concentration at t0, and A is the monolayer surface area. The efflux ratio is calculated by dividing the P_{app} B-A by the P_{app} A-B.

Chemistry. Complete experimental methods (synthesis and characterization) for each target compound and intermediates are in the Supporting Information. Purification of the final compounds was carried out either using prepacked silica gel cartridges (Analogix, Biotage or ISCO) or a reverse phase C18 column. ^{1}H and ^{13}C NMR spectra were recorded on Bruker spectrometers. NMR chemical shifts (δ) are quoted in parts per million [ppm] and referenced to the residual solvent peak. The purity of all compounds was determined to be >95% by analytical HPLC.

3-(3-methoxybenzyl)piperidine (**2**). Purchased from BioBlocks, #BP039-1. Yellow Powder. ^{1}H NMR (400 MHz, DMSO-d_6): δ = 8.90 (d, *J* = 110.5 Hz, 2H), 7.20 (t, *J* = 7.8 Hz, 1H), 6.74 (m, *J* = 7.6, 6.7 Hz, 3H), 3.71 (s, 3H), 3.32 (s, 2H), 3.14 (d, *J* = 11.5 Hz, 1H), 3.00 (d, *J* = 11.3 Hz, 1H), 2.81–2.59 (m, 1H), 1.96 (s, 1H), 1.82–1.46 (m, 4H), 1.15 (q, *J* = 11.7, 11.1 Hz, 1H). ^{13}C NMR (100 MHz, DMSO-d_6): δ = 159.7, 140.9, 129.8, 121.6, 115.1, 111.9, 55.4, 47.9, 43.7, 35.0, 28.6, 22.0. LC-MS (m/z): 206.0 $[M+H]^+$.

3-benzylpiperidine (**3**), **3-(2-methoxybenzyl)piperidine** (**4**), and **3-(4-methoxybenzyl) piperidine** (**5**) are commercially available.

3-(4-Fluoro-3-methoxybenzyl)piperidine (**6**). A solution of *tert*-butyl 3-(4-fluoro-3-methoxybenzyl)piperidine-1-carboxylate (compound **6-1** in the Supporting Information , 30 mg, 0.093 mmol) in 4M HCl/dioxane (0.5 mL) was stirred at r.t. for 3 h. After removing the solvent under reduced pressure, the residue was purified with HPLC to yield compound **6** (13.7 mg, 42% yield). ^{1}H NMR (400 MHz, MeOD-d_4): δ = 7.05–7.00 (m, 2H), 6.79 (br. s., 1H), 3.85 (s, 3H), 3.26–3.23 (m, 1H), 2.89 (br. s., 1H), 2.77–2.54 (m, 3H), 2.05 (br. s., 1H), 1.97–1.77 (m, 2H), 1.70–1.67 (m, 1H), 1.42–1.22 (m, 1H). LC-MS (m/z): 224.1 $[M+H]^+$.

3-(Benzofuran-7-ylmethyl)piperidine (**7**). HCl/dioxane (4M, 0.2 mL) was added to a solution of *tert*-butyl 3-(benzofuran-7-ylmethyl)piperidine-1-carboxylate (compound **7-1** in the Supporting Information, 21 mg, 0.067 mmol) in DCM. The mixture was stirred at r.t. for 3 h. The mixture was evaporated to dryness to give compound **7** as its HCl salt (18.2 mg, quantitative). ^{1}H NMR (400 MHz, MeOD-d_4): δ = 7.85–7.72 (m, 1H), 7.51 (d, *J* = 7.53 Hz, 1H), 7.25–7.16 (m, 1H), 7.16–7.09 (m, 1H), 6.90–6.78 (m, 1H), 3.23 (d, *J* = 11.80 Hz, 1H), 3.05–2.84 (m, 3H), 2.76 (t, *J* = 12.30 Hz, 1H), 2.36–2.20 (m, 1H), 1.98–1.82 (m, 2H), 1.80–1.64 (m, 1H), 1.45–1.25 (m, 1H). LC-MS (m/z): 216.2 $[M+H]^+$.

3-(Benzofuran-4-ylmethyl)piperidine (**8**). To a solution of *tert*-butyl 3-(benzofuran-4-ylmethyl)piperidine-1-carboxylate (compound **8-1** in the Supporting Information, 57 mg, 0.181mmol) in DCM was added HCl/dioxane (4M, 0.2 mL). The mixture was stirred at r.t. for 3 h. The mixture was concentrated under reduced pressure to give compound **8** as its HCl salt (47.8 mg, quantitative). ^{1}H NMR (400 MHz, MeOD-d_4): δ = 7.85–7.70 (m, 1H), 7.38 (d, *J* = 8.28 Hz, 1H), 7.24 (t, *J* = 7.78 Hz, 1H), 7.06 (d, *J* = 7.28 Hz, 1H), 6.98 (s, 1H), 3.27–3.37 (m, 1H), 3.24

(d, *J* = 11.80 Hz, 1H), 2.83–2.99 (m, 3H), 2.79–2.73 (m, 1H), 2.23–2.17 (m, 1H), 1.91–1.82 (m, 2H), 1.77–1.60 (m, 1H), 1.46–1.21 (m, 1H). LC-MS (m/z): 216.1 $[M+H]^+$.

3-(Benzo[d][1,3]dioxol-4-ylmethyl)piperidine (**9**). To a solution of *tert*-butyl 3-(benzo[d][1,3]dioxol-4-ylmethyl)piperidine-1-carboxylate (**9-1** in the Supporting Information, 26 mg, 0.081 mmol) in DCM was added HCl/dioxane (4M, 0.2 ml). The mixture was stirred at r.t. for 3 h. The mixture was concentrated under reduced pressure and dried in vacuo to afford compound **9** as its HCl salt (21.6 mg, 99%). ^{1}H NMR (400 MHz, MeOD-d_4): δ = 6.75–6.84 (m, 1H), 6.63–6.75 (m, 2H), 5.93 (s, 2H), 3.35 (d, *J* = 3.01 Hz, 1H), 3.26 (d, *J* = 11.04 Hz, 1H), 2.90 (t, *J* = 12.17 Hz, 1H), 2.50–2.78 (m, 3H), 2.15 (dtd, *J* = 15.00, 7.44, 7.44, 3.76 Hz, 1H), 1.82–1.99 (m, 2H), 1.61–1.80 (m, 1H), 1.21–1.44 (m, 2H). LC-MS (m/z): 220.2 $[M+H]^+$.

3-(3-methoxybenzyl)piperidine-1-carboximidamide (**10**). A mixture of 3-(3-methoxybenzyl)piperidine (**10-1** in the Supporting Information, 40 mg, 0.2 mmol), 1*H*-pyrazole-1-carboximidamide (**10-2** in the Supporting Information, 110 mg, 1 mmol) and DIPEA (129 mg, 1 mmol) in DMF (3 mL) was stirred at r.t. until consumption of starting material as monitored by LC-MS. The reaction mixture was purified by preparative HPLC to afford the title compound **10** as a white solid (39 mg, 81% yield). ^{1}H NMR (400 MHz, MeOD-d_4): δ = 7.21 (t, *J* = 8.0 Hz, 1H), 6.76–6.80 (m, 3H), 3.76–3.80 (m, 5H), 3.04–3.11 (m, 1H), 2.83–2.89 (m, 1H), 2.65–2.70 (m, 1H), 2.42–2.48 (m, 1H), 1.77–1.89 (m, 3H), 1.49–1.53 (m, 1H), 1.25–1.32 (m, 1H); LC-MS (m/z): 248.2 $[M+H]^+$.

3-(Benzofuran-7-ylmethyl)piperidine-1-carboximidamide triflate (**11**). The title compound **11** was prepared similar to the preparation of compound **10** starting from compound 7-bromobenzofuran. ^{1}H NMR (400 MHz, DMSO-d_6): δ = 7.99 (d, *J* = 2.0 Hz, 1H), 7.52 (dd, *J* = 0.8, 7.6 Hz, 1H), 7.34–7.38 (m, 4H), 7.11–7.22 (m, 2H), 6.96 (d, *J* = 2.0 Hz, 1H), 3.85 (d, *J* =

12.4 Hz, 1H), 3.72 (d, *J* = 13.6 Hz, 1H), 2.85–3.05 (m, 3H), 2.67–2.74 (m, 1H), 1.95–1.99 (m, 1H), 1.54–1.68 (m, 2H), 1.20–1.37 (m, 2H); LC-MS (m/z): 258.2 $[M+H]^+$.

3-(Benzofuran-4-ylmethyl)piperidine-1-carboximidamide triflate (**12**). The title compound **12** was prepared similar to the preparation of compound **10** starting from compound 4-bromobenzofuran. ^{1}H NMR (400 MHz, DMSO-d_6): δ = 7.99 (d, *J* = 2.0 Hz, 1H), 7.45 (d, *J* = 8.4 Hz, 1H), 7.20–7.32 (m, 5H), 7.10 (d, *J* = 1.2 Hz, 1H), 7.05 (d, *J* = 7.2 Hz, 1H), 3.86 (d, *J* = 12.4 Hz, 1H), 3.75 (d, *J* = 13.6 Hz, 1H), 2.81–3.00 (m, 3H), 2.59–2.66 (m, 1H), 1.83–1.86 (m, 1H), 1.54–1.67 (m, 2H), 1.20–1.34 (m, 2H); LC-MS (m/z): 258.2 $[M+H]^+$.

3-(Benzofuran-4-ylmethyl)piperidine-1-carboxamide (**13**). To a solution of DCM (4.5 mL) was added 3-(benzofuran-4-ylmethyl)piperidine hydrochloride (15 mg, 0.059 mmol) and triethylamine (30 mg, 0.297 mmol). After stirring for 30 minutes at r.t., isocyanatotrimethylsilane (23 mg, 0.2 mmol) was added and stirring was coninued for 1 h. The solvent was removed under reduced pressure and the residue was purified by preparative HPLC to afford the title compound **13** as a white solid (9 mg, 50% yield). ^{1}H NMR (400MHz, MeOD-d_4): δ = 7.74–7.73 (m, 1H), 7.36–7.34 (m, 1H), 7.24–7.20 (t, 1H), 7.06–7.04 (d, 1H), 6.95–6.94 (m, 1H), 3.99–3.95 (m, 1H), 3.85–3.82 (m, 1H), 2.90–2.83 (m, 2H), 2.75–2.62 (m, 2H), 1.89–1.76 (m, 1H), 1.58–1.62 (m, 2H), 1.46–1.35 (m, 2H). LC-MS (m/z): 259.0 $[M+H]^+$.

3-(Benzo[d][1,3]dioxol-5-ylmethyl)piperidine-1-carboximidamide (**14**). A mixture of 3-(benzo[d][1,3]dioxol-5-ylmethyl)piperidine hydrochloride (**14-2** in the Supporting Information, 60 mg, 0.27 mmol), 1*H*-pyrazole-1-carboximidamide (150 mg, 1.37 mmol) and DIPEA (177 mg, 1.37 mmol) in DMF (5 mL) was stirred at r.t. until complete consumption of starting material as monitored by LC-MS. The mixture was purified by preparative HPLC to afford the title compound **14** as a white solid (54 mg, 88% yield). ^{1}H NMR (400 MHz, MeOD-d_4): δ = 6.67–

6.80 (m, 3H), 5.93 (dd, *J* = 1.2, 4.0 Hz, 2H), 3.80 (t, *J* = 1.6 Hz,, 2H), 3.01–3.08 (m, 1H), 2.81–2.87 (m, 1H), 2.63–2.68 (m, 1H), 2.48–2.53 (m, 1H), 1.75–1.98(m, 3H), 1.31–1.54 (m, 2H); LC-MS (m/z): 262.2 $[M+H]^+$.

6-(Benzofuran-4-ylmethyl)-5,6,7,8-tetrahydroimidazo[1,5-a]pyridin-3-amine (**15**). To a solution of 6-(benzofuran-4-ylmethyl)imidazo[1,5-a]pyridin-3-amine (**15-7** in the Supporting Information, 20 mg, 0.053 mmol) in MeOH (10 mL) was added Pd/C (0.564 mg, 5.30 μmol) and three drops of concentrated hydrochloride acid. The mixture was stirred at 25 °C for 2 h and the progress of the reaction monitored by LC-MS. The mixture was cooled to r.t. and filtered through Celite. The filtrate was concentrated under reduced pressure. The residue was purified by preparative HPLC to give **15** as a white powder. ^{1}H NMR (400 MHz, MeOD-d_4): δ = 7.77 (s, 1H), 7.41–7.38 (m, 1H), 7.31–7.21 (m, 1H), 7.16–7.10 (m, 1H), 6.95 (s, 1H), 6.55 (s, 1H), 3.90–3.82 (m, 1H), 3.40–3.30 (m, 1H), 3.07–2.95 (m, 2H), 2.95–2.85 (m, 1H), 2.67–2.51 (m, 1H), 2.49–2.40 (m, 1H), 2.05–1.95 (m, 1H), 1.62–1.50 (m, 1H). LC-MS (m/z): 268 $[M+H]^+$.

6-(Benzo[d][1,3]dioxol-4-ylmethyl)-5,6,7,8-tetrahydroimidazo[1,5-a]pyridin-3-amine (**16**). To a solution of 6-(benzo[d][1,3]dioxol-4-ylmethyl)imidazo[1,5-a]pyridin-3-amine (**16-9** in the Supporting Information, 20 mg, 0.075 mmol) in MeOH (10 mL) was added Pd/C (7.96 mg, 7.48 μmol) and three drops of concentrated hydrochloride acid. The resulting mixture was stirred at 50 °C for 4 h, cooled to r.t. and filtered through Celite. The filtrate was concentrated under reduced pressure. The residue was purified by preparative HPLC to give compound **16** as a white powder. ^{1}H NMR (400 MHz, MeOD-d_4): δ = 6.83–6.70 (m, 3H), 6.55 (s, 1H), 6.05–5.95 (m, 2H), 3.92–3.86 (m, 1H), 3.40–3.30 (m, 1H), 2.95–2.85 (m, 1H), 2.80–2.75 (m, 2H), 2.71–2.61 (m, 1H), 2.35–2.45 (m, 1H), 2.05–1.95 (m, 1H), 1.62–1.50 (m, 1H). LC-MS (m/z): 272 $[M+H]^+$.

(Benzo[d][1,3]dioxol-4-ylmethyl)-1-isopropyl-5,6,7,8-tetrahydroimidazo[1,5-a]pyridin-3-amine (**17**). A mixture of 6-(benzo[d][1,3]dioxol-4-ylmethyl)-1-isopropylimidazo[1,5-a]pyridin-3-amine (**17-4** in the Supporting Information, 50 mg, 0.16 mmol) and Pd/C (25 mg, 0.235 mmol) in MeOH (30 mL) containing HCl/dioxane (4M, 0.1 mL) was stirred for 5 h at 25 °C under hydrogen atmosphere. The reaction mixture was concentrated under reduced pressure and the residue was purified by preparative HPLC to afford compound **17** as a white solid (20 mg, 29% yield). ^{1}H NMR (400 MHz, MeOD-d_4): δ = 6.89–6.80 (m, 1H), 6.75–6.65 (m, 2H), 6.00–6.92 (m, 2H), 3.89–3.80 (m, 1H), 3.30–3.25 (m, 1H), 2.95–2.82 (m, 2H), 2.75–2.65 (m, 2H), 2.61–2.51 (m, 1H), 2.40–2.30 (m, 1H), 2.05–1.95 (m, 1H), 1.58–1.46 (m, 1H), 1.24 (t, *J* = 7 Hz, 6H). LC-MS (m/z): 314 $[M+H]^+$.

6-(2-fluorobenzyl)-1-isopropyl-5,6,7,8-tetrahydroimidazo[1,5-a]pyridin-3-amine (**18**). Compound **18** was prepared similar to the preparation of compound **19**. ^{1}H NMR (400 MHz, MeOD-d_4): δ = 7.25–7.33 (m, 2H), 7.06–7.18 (m, 2H), 4.58 (s, 1H), 3.84 (ddd, *J* = 12.04, 5.22, 1.03 Hz, 1H), 3.23–3.28 (m, 1H), 2.76–2.96 (m, 4H), 2.52 (ddd, *J* = 16.52, 11.21, 5.62 Hz, 1H), 2.23–2.34 (m, 1H), 1.93–2.02 (m, 1H), 1.50 (dtd, *J* = 13.38, 11.22, 11.22, 5.26 Hz, 1H), 1.21 (t, *J* = 7.09 Hz, 6H). LC-MS (m/z): 288.3 $[M+H]^+$.

6-(2-fluoro-5-methoxybenzyl)-1-isopropyl-5,6,7,8-tetrahydroimidazo[1,5-a]pyridin-3-amine (**19**). To a solution of 6-(2-fluoro-5-methoxybenzyl)-1-isopropylimidazo[1,5-a]pyridin-3-amine (**19-6** in the Supporting Information, 90 mg, 0.287 mmol) in MeOH (50.5 mL) was added Pd/C (45.5 mg, 0.428 mmol) and 4M HCl in dioxane (0.168 mL). The mixture was purged twice with hydrogen and then stirred under hydrogen atmosphere (balloon) ovenight. The mixture was filtered through Celite, rinsed with DCM and the filtrate was concentrated under reduced pressure. The residue was purified by reverse phase HPLC providing **19** as its trifluoroacetic acid

salt as a white solid (7.7 mg, 6% yield). ^{1}H NMR (400 MHz, MeOD-d_4): δ = 7.01 (t, *J* = 9.17 Hz, 1H), 6.75–6.88 (m, 2H), 3.83 (ddd, *J* = 12.04, 5.15, 0.90 Hz, 1H), 3.78 (s, 3H), 3.27 (dd, *J* = 11.98, 10.32 Hz, 1H), 2.82–2.96 (m, 2H), 2.75 (d, *J* = 7.24 Hz, 2H), 2.47–2.57 (m, 1H), 2.24–2.34 (m, 1H), 1.94–2.02 (m, 1H), 1.50 (dtd, *J* = 13.33, 11.17, 11.17, 5.31 Hz, 1H), 1.22 (t, *J* = 7.02 Hz, 6H). LC-MS (m/z): 318.2 $[M+H]^+$.

ASSOCIATED CONTENT

Supporting Information. Three figures, two tables and complete experimental methods are supplied as Supporting Information, as well as Molecular Formula Strings.

PDB ID Codes

PDB accession codes are: EED in complex with compound **2**, 5U5K; compound **14**, 5U5T; compound **16**, 5U62; compound **19**, 5U5H. Authors will release the atomic coordinates and experimental data upon article publication.

AUTHOR INFORMATION

Corresponding Author

*andreas.lingel@novartis.com, phone: +41 79 630 48 15

#for compound requests: dirksen.bussiere@novartis.com, phone: +1 510 879 9505

Present Addresses

[§]Novartis Institutes for BioMedical Research, 250 Massachusetts Avenue, Cambridge, Massachusetts 02139, United States

[&]Ideaya Biosciences, 280 Utah Avenue, South San Francisco, CA 94080, United States

[¶]Novartis Institutes for BioMedical Research, Novartis Campus, 4056 Basel, Switzerland

[¥]Array BioPharma, 3200 Walnut Street, Boulder, CO 80301, United States

ACKNOWLEDGMENT

We thank the staff of Sector 5 at the Advanced Light Source and the staff of Crystallographic Consulting, LLC, for assistance in collecting X-ray crystallographic data. The Advanced Light Source is supported by the Director, Office of Science, Office of Basic Energy Sciences, of the U.S. Department of Energy under Contract No. DE-AC02-05CH11231. We also thank Laura Tandeske for subcloning of the His-TEV-EED$_{76-441}$ construct, Weiping Jia, Linhong Yang and Suzanne Skolnik for the pK_a measurements, as well as Colin Lorentzen and Linda Xiao for providing the Caco-2 permeability measurements. Furthermore, we thank Karin Briner, Counde Oyang, En Li, Emma Lees, and William Sellers for their support.

ABBREVIATIONS USED

NMR, nuclear magnetic resonance; DMSO, dimethyl sulfoxide; DTT, dithiothreitol; HAC, heavy atom count; LE, ligand efficiency; LipE, lipophilic efficiency; SAR, structure-activity relationship; PRC, Polycomb repressive complex; EED, Embryonic ectoderm development; HSQC, Heteronuclear single quantum coherence; IMAC, immobilized metal affinity chromatography; n.d., not determined; r.t., room temperature; h, hour(s)

REFERENCES

(1) Margueron, R.; Reinberg, D. The Polycomb Complex PRC2 and Its Mark in Life. *Nature* **2011**, *469*, 343–349.

(2) Cao, R.; Zhang, Y. SUZ12 Is Required for Both the Histone Methyltransferase Activity and the Silencing Function of the EED-EZH2 Complex. *Mol. Cell* **2004**, *15*, 57–67.

(3) Ciferri, C.; Lander, G. C.; Maiolica, A.; Herzog, F.; Aebersold, R.; Nogales, E. Molecular Architecture of Human Polycomb Repressive Complex 2. *Elife* **2012**, *1*,e00005.

(4) Brooun, A.; Gajiwala, K. S.; Deng, Y.-L.; Liu, W.; Bolaños, B.; Bingham, P.; He, Y.-A.; Diehl, W.; Grable, N.; Kung, P.-P.; Sutton, S.; Maegley, K. A.; Yu, X.; Stewart, A. E. Polycomb Repressive Complex 2 Structure with Inhibitor Reveals a Mechanism of Activation and Drug Resistance. *Nat. Commun.* **2016**, *7*,11384.

(5) Jiao, L.; Liu, X. Structural Basis of Histone H3K27 Trimethylation by an Active Polycomb Repressive Complex 2. *Science* **2015**, *350*, aac4383–aac4383.

(6) Justin, N.; Zhang, Y.; Tarricone, C.; Martin, S. R.; Chen, S.; Underwood, E.; De Marco, V.; Haire, L. F.; Walker, P. a; Reinberg, D.; Wilson, J. R.; Gamblin, S. J. Structural Basis of Oncogenic Histone H3K27M Inhibition of Human Polycomb Repressive Complex 2. *Nat. Commun.* **2016**, *7*,11316.

(7) McCabe, M.T.; Creasy, C. L. EZH2 as a Potential Target in Cancer Therapy. *Epigenomics* **2014**, *6*, 341–351.

(8) Varambally, S.; Dhanasekaran, S. M.; Zhou, M.; Barrette, T. R.; Kumar-Sinha, C.; Sanda, M. G.; Ghosh, D.; Pienta, K. J.; Sewalt, R. G.; Otte, A. P.; Rubin, M. A.; Chinnaiyan, A. M. The Polycomb Group Protein EZH2 Is Involved in Progression of Prostate Cancer. *Nature* **2002**, *419*, 624-629.

(9) Morin, R. D.; Johnson, N. A.; Severson, T. M.; Mungall, A. J.; An, J.; Goya, R.; Paul, J. E.; Boyle, M.; Woolcock, B. W.; Kuchenbauer, F.; Yap, D.; Humphries, R. K.; Griffith, O. L.; Shah, S.; Zhu, H.; Kimbara, M.; Shashkin, P.; Charlot, J. F.; Tcherpakov, M.; Corbett, R.; Tam, A.; Varhol, R.; Smailus, D.; Moksa, M.; Zhao, Y.; Delaney, A.; Qian, H.; Birol, I.; Schein, J.; Moore, R.; Holt, R.; Horsman, D. E.; Connors, J. M.; Jones, S.; Aparicio, S.; Hirst, M.; Gascoyne, R. D.; Marra, M. A. Somatic Mutations Altering EZH2 (Tyr641) in Follicular and Diffuse Large B-Cell Lymphomas of Germinal-Center Origin. *Nat. Genet.* **2010**, *42*, 181–185.

(10) Takawa, M.; Masuda, K.; Kunizaki, M.; Daigo, Y.; Takagi, K.; Iwai, Y.; Cho, H.-S.; Toyokawa, G.; Yamane, Y.; Maejima, K.; Field, H. I.; Kobayashi, T.; Akasu, T.; Sugiyama, M.; Tsuchiya, E.; Atomi, Y.; Ponder, B. A. J.; Nakamura, Y.; Hamamoto, R. Validation of the Histone Methyltransferase EZH2 as a Therapeutic Target for Various Types of Human Cancer and as a Prognostic Marker. *Cancer Sci.* **2011**, *102*, 1298–1305.

(11) Knutson, S. K.; Wigle, T. J.; Warholic, N. M.; Sneeringer, C. J.; Allain, C. J.; Klaus, C. R.; Sacks, J. D.; Raimondi, A.; Majer, C. R.; Song, J.; Scott, M. P.; Jin, L.; Smith, J. J.; Olhava, E. J.; Chesworth, R.; Moyer, M. P.; Richon, V. M.; Copeland, R. a; Keilhack, H.; Pollock, R. M.; Kuntz, K. W. A Selective Inhibitor of EZH2 Blocks H3K27 Methylation and Kills Mutant Lymphoma Cells. *Nat. Chem. Biol.* **2012**, *8*, 890–896.

(12) McCabe, M. T.; Ott, H. M.; Ganji, G.; Korenchuk, S.; Thompson, C.; Van Aller, G. S.; Liu, Y.; Graves, A. P.; Della Pietra, A.; Diaz, E.; LaFrance, L. V; Mellinger, M.; Duquenne, C.; Tian, X.; Kruger, R. G.; McHugh, C. F.; Brandt, M.; Miller, W. H.; Dhanak, D.; Verma, S. K.; Tummino, P. J.; Creasy, C. L. EZH2 Inhibition as a Therapeutic Strategy for Lymphoma with EZH2-Activating Mutations. *Nature* **2012**, *492*, 108–112.

(13) Konze, K. D.; Ma, A.; Li, F.; Barsyte-Lovejoy, D.; Parton, T.; Macnevin, C. J.; Liu, F.; Gao, C.; Huang, X.; Kuznetsova, E.; Rougie, M.; Jiang, A.; Pattenden, S. G.; Norris, J. L.; James, L. I.; Roth, B. L.; Brown, P. J.; Frye, S. V; Arrowsmith, C. H.; Hahn, K. M.; Wang, G. G.; Vedadi, M.; Jin, J. An Orally Bioavailable Chemical Probe of the Lysine Methyltransferases EZH2 and EZH1. *ACS Chem. Biol.* **2013**, *8*, 324-1334.

(14) Verma, S. K.; Tian, X.; Lafrance, L. V; Suarez, D. P.; Newlander, K. A.; Romeril, S. P.; Burgess, J. L.; Grant, S. W.; Brackley, J. A.; Graves, A. P.; Scherzer, D. A.; Shu, A.; Thompson, C.; Ott, H. M.; Aller, G. S. Van; Machutta, C. A.; Diaz, E.; Jiang, Y.; Johnson, N. W.; Knight, S. D.; Kruger, R. G.; McCabe, M. T.; Dhanak, D.; Tummino, P. J.; Creasy, C. L.; Miller, W. H. Identification of Potent, Selective, Cell-Active Inhibitors of the Histone Lysine Methyltransferase EZH2. *ACS Med. Chem. Lett.* **2012**, *3*, 1091-1096.

(15) Qi, W.; Chan, H.; Teng, L.; Li, L.; Chuai, S.; Zhang, R.; Zeng, J.; Li, M.; Fan, H.; Lin, Y.; Gu, J.; Ardayfio, O.; Zhang, J. H.; Yan, X.; Fang, J.; Mi, Y.; Zhang, M.; Zhou, T.; Feng, G.; Chen, Z.; Li, G.; Yang, T.; Zhao, K.; Liu, X.; Yu, Z.; Lu, C. X.; Atadja, P.; Li, E. Selective Inhibition of Ezh2 by a Small Molecule Inhibitor Blocks Tumor Cells Proliferation. *Proc. Natl. Acad. Sci. U. S. A.* **2012**, *109*, 21360-21365.

(16) Garapaty-Rao, S.; Nasveschuk, C.; Gagnon, A.; Chan, E. Y.; Sandy, P.; Busby, J.; Balasubramanian, S.; Campbell, R.; Zhao, F.; Bergeron, L.; Audia, J. E.; Albrecht, B. K.; Harmange, J.-C.; Cummings, R.; Trojer, P. Identification of EZH2 and EZH1 Small Molecule Inhibitors with Selective Impact on Diffuse Large B Cell Lymphoma Cell Growth. *Chem. Biol.* **2013**, *20*, 1329–1339.

(17) Nasveschuk, C. G.; Gagnon, A.; Garapaty-Rao, S.; Balasubramanian, S.; Campbell, R.; Lee, C.; Zhao, F.; Bergeron, L.; Cummings, R.; Trojer, P.; Audia, J. E.; Albrecht, B. K.; Harmange, J. P. Discovery and Optimization of Tetramethylpiperidinyl Benzamides as Inhibitors of EZH2. *ACS Med. Chem. Lett.* **2014**, *5*, 378–383.

(18) Gehling, V. S.; Vaswani, R. G.; Nasveschuk, C. G.; Duplessis, M.; Iyer, P.; Balasubramanian, S.; Zhao, F.; Good, A. C.; Campbell, R.; Lee, C.; Dakin, L. A.; Cook, A. S.; Gagnon, A.; Harmange, J.-C.; Audia, J. E.; Cummings, R. T.; Normant, E.; Trojer, P.; Albrecht, B. K. Discovery, Design, and Synthesis of Indole-Based EZH2 Inhibitors. *Bioorg. Med. Chem. Lett.* **2015**, *25*, 3644–3649.

(19) Kim, K. H.; Roberts, C. W. M. Targeting EZH2 in Cancer. *Nat. Med.* **2016**, *22*, 128–134.

(20) Kim, W.; Bird, G. H.; Neff, T.; Guo, G.; Kerenyi, M. A.; Walensky, L. D.; Orkin, S. H. Targeted Disruption of the EZH2-EED Complex Inhibits EZH2-Dependent Cancer. *Nat. Chem. Biol.* **2013**, *9*, 643–650.

(21) Han, Z.; Xing, X.; Hu, M.; Zhang, Y.; Liu, P.; Chai, J. Structural Basis of EZH2 Recognition by EED. *Structure* **2007**, *15*, 1306–1315.

(22) Margueron, R.; Justin, N.; Ohno, K.; Sharpe, M. L.; Son, J.; Drury, W. J.; Voigt, P.; Martin, S. R.; Taylor, W. R.; De Marco, V.; Pirrotta, V.; Reinberg, D.; Gamblin, S. J. Role of the Polycomb Protein EED in the Propagation of Repressive Histone Marks. *Nature* **2009**, *461*, 762–767.

(23) Xu, C.; Bian, C.; Yang, W.; Galka, M.; Ouyang, H.; Chen, C.; Qiu, W.; Liu, H.; Jones, A. E.; MacKenzie, F.; Pan, P.; Li, S. S.-C.; Wang, H.; Min, J. Binding of Different Histone Marks Differentially Regulates the Activity and Specificity of Polycomb Repressive Complex 2 (PRC2). *Proc. Natl. Acad. Sci. U. S. A.* **2010**, *107*, 19266–19271.

(24) Details of the biochemical high throughput screen (assays and compound sets) and biochemical characterization (competition studies with SAM, H3K27Me0 and H3K27Me3) as well as the co-structure of EED with compound **1** (PDB accession code: 5H17) are described in a separate manuscript currently under review.

(25) Kozakov, D.; Hall, D. R.; Jehle, S.; Luo, L.; Ochiana, S. O.; Jones, E. V; Pollastri, M.; Allen, K. N.; Whitty, A.; Vajda, S. Ligand Deconstruction: Why Some Fragment Binding Positions Are Conserved and Others Are Not. *Proc. Natl. Acad. Sci. U. S. A.* **2015**, *112*, E2585-E2594.

(26) Chen, H.; Zhou, X.; Wang, A.; Zheng, Y.; Gao, Y.; Zhou, J. Evolutions in Fragment-Based Drug Design: The Deconstruction-Reconstruction Approach. *Drug Discovery Today* **2015**, *20*, 105–113.

(27) Optimization of another chemical series will be described in detail in a separate manuscript currently in revision.

(28) Wilson, B. G.; Wang, X.; Shen, X.; McKenna, E. S.; Lemieux, M. E.; Cho, Y.-J.; Koellhoffer, E. C.; Pomeroy, S. L.; Orkin, S. H.; Roberts, C. W. M. Epigenetic Antagonism between Polycomb and SWI/SNF Complexes during Oncogenic Transformation. *Cancer Cell* **2010**, *18*, 316–328.

(29) BioLoom database; BioByte Corp., 201 W. 4th St., #204, Claremont, CA 91711-4707; http://www.biobyte.com/bb/prod/bioloom.html

(30) Müller, K.; Faeh, C.; Diederich, F. Fluorine in Pharmaceuticals: Looking Beyond Intuition. *Science* **2007**, *317*, 1881–1887.

(31) Gibaja, V.; Shen, F.; Harari, J.; Korn, J.; Ruddy, D.; Saenz-Vash, V.; Zhai, H.; Rejtar, T.; Paris, C. G.; Yu, Z.; Lira, M.; King, D.; Qi, W.; Keen, N.; Hassan, A. Q.; Chan, H. M. Development of Secondary Mutations in Wild-Type and Mutant EZH2 Alleles Cooperates to Confer Resistance to EZH2 Inhibitors. *Oncogene* **2016**, *35*, 558–566.

(32) Baker, T.; Nerle, S.; Pritchard, J.; Zhao, B.; Rivera, V. M.; Garner, A.; Gonzalvez, F. Acquisition of a Single EZH2 D1 Domain Mutation Confers Acquired Resistance to EZH2-Targeted Inhibitors. *Oncotarget* **2015**, *6*, 32646– 32655.

(33) Emsley, P.; Lohkamp, B.; Scott, W. G.; Cowtan, K. Features and Development of Coot. *Acta Crystallogr., Sect. D: Biol. Crystallogr.* **2010**, *66*, 486–501.

(34) Bricogne, G.; Blanc, E.; Brandl, M.; Flensburg, C.; Keller, P.; Paciorek, W.; Roversi, P.; Sharff, A.; Smart, O. S.; Vonrhein, C.; Womack, T. O. (2016), BUSTER version 2.11.6., Cambridge, United Kingdom: Global Phasing Ltd.

(35) Adams, P. D.; Afonine, P. V; Bunkóczi, G.; Chen, V. B.; Davis, I. W.; Echols, N.; Headd, J. J.; Hung, L.-W.; Kapral, G. J.; Grosse-Kunstleve, R. W.; McCoy, A. J.; Moriarty, N. W.; Oeffner, R.; Read, R. J.; Richardson, D. C.; Richardson, J. S.; Terwilliger, T. C.; Zwart, P. H. PHENIX: A Comprehensive Python-Based System for Macromolecular Structure Solution. *Acta Crystallogr., Sect. D: Biol. Crystallogr.* **2010**, *66*, 213–221.

(36) Li, S.; Gu, X. J.; Hao, Q.; Fan, H.; Li, L.; Zhou, S.; Zhao, K.; Chan, H. M.; Wang, Y. K. A Liquid Chromatography/mass Spectrometry-Based Generic Detection Method for Biochemical Assay and Hit Discovery of Histone Methyltransferases. *Anal. Biochem.* **2013**, *443*, 214–221.

(37) Gedeck, P.; Lu, Y.; Skolnik, S.; Rodde, S.; Dollinger, G.; Jia, W.; Berellini, G.; Vianello, R.; Faller, B.; Lombardo, F. Benefit of Retraining pKa Models Studied Using Internally Measured Data. *J. Chem. Inf. Model.* **2015**, *55*, 1449–1459.

Table of Contents Graphic

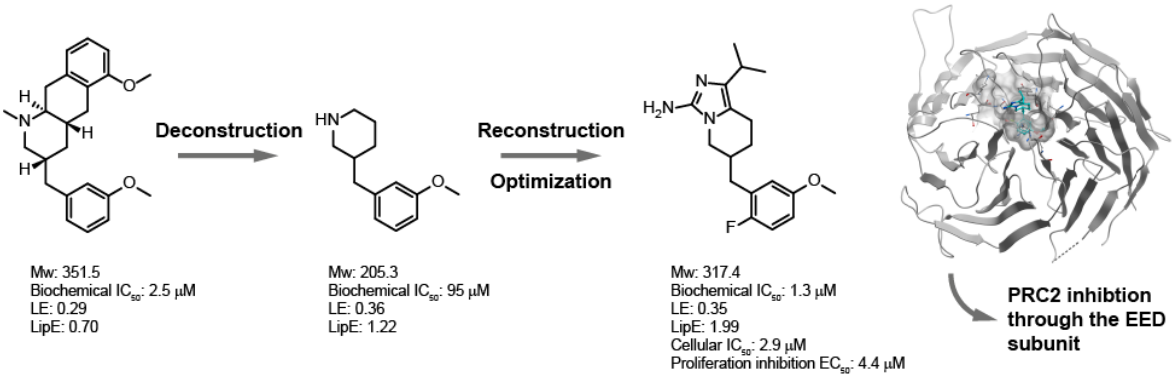

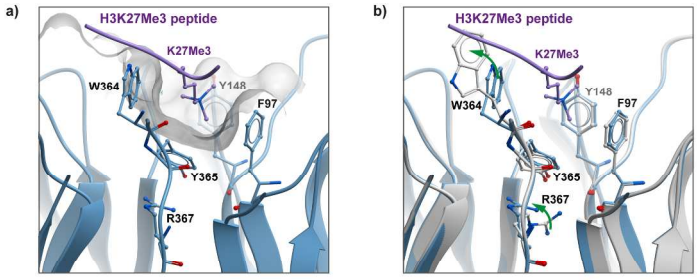

240x103mm (300 x 300 DPI)

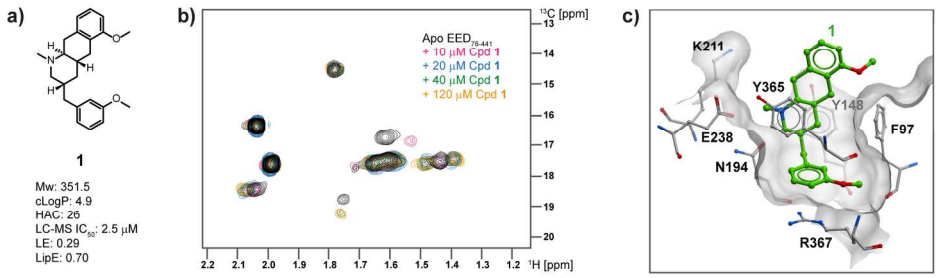

179x58mm (300 x 300 DPI)

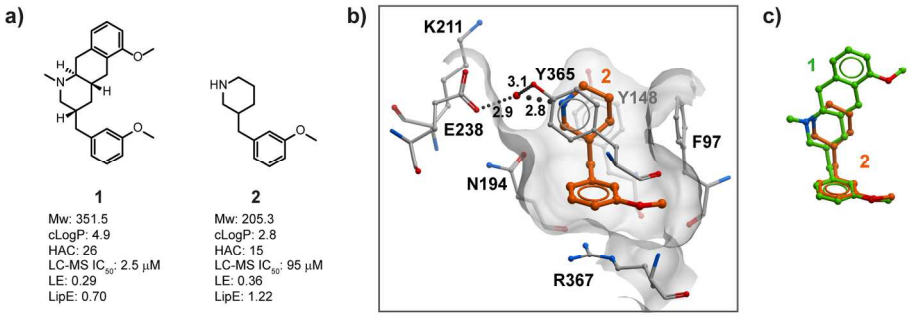

163x61mm (300 x 300 DPI)

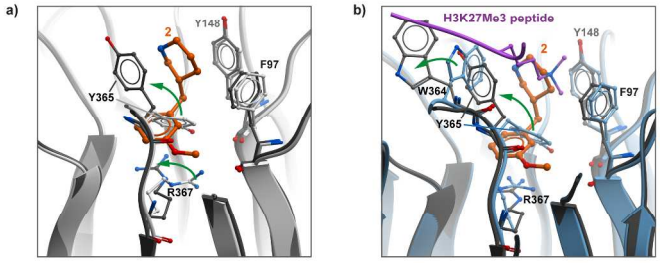

254x123mm (300 x 300 DPI)

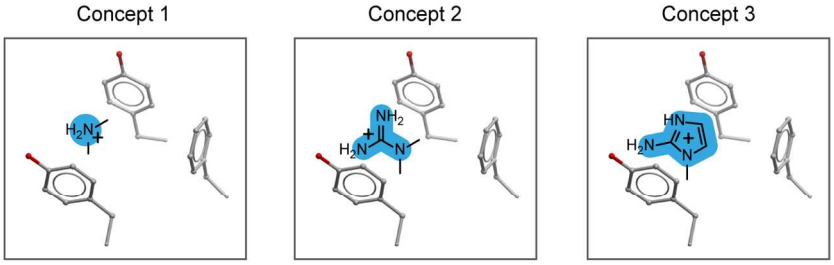

	Concept 1	Concept 2	Concept 3
Type of charge	Point charge	Delocalized charge	Delocalized charge
Stacking interaction	No pi stacking	Pi stacking	Aromatic pi stacking
Example	Aliphatic amine	Guanidinium	2-Aminoimidazole

154x59mm (300 x 300 DPI)

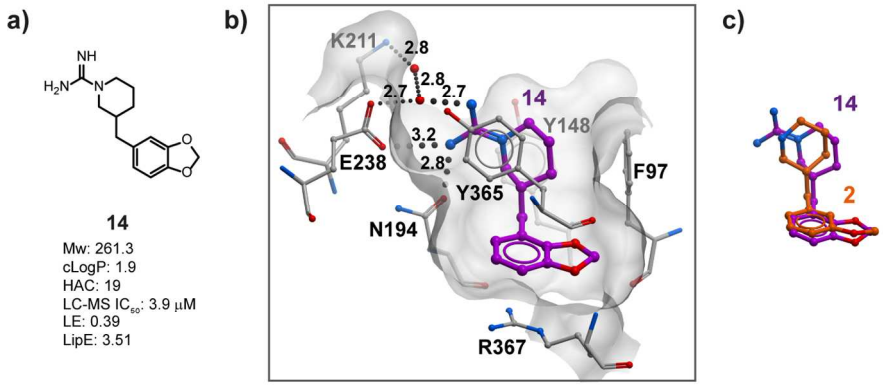

137x59mm (300 x 300 DPI)

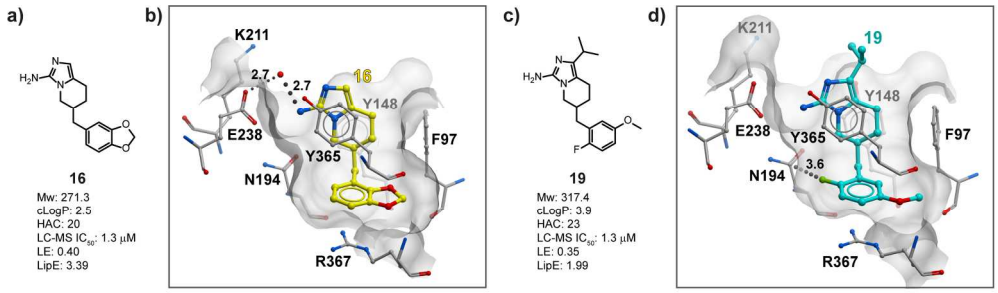

185x56mm (300 x 300 DPI)